NDT&E International 145 (2024) 103120

Contents lists available at ScienceDirect

NDT and E International

journal homepage: www.elsevier.com/locate/ndteint

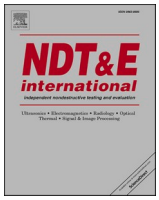

A feasibility study on phase characterisation of nickel-based superalloys using ultrasound

Jennifer H. Jobling [a,*], Edward A. Saunders [b], Tim Barden [b], Michael J.S. Lowe [a], Bo Lan [a,**]

[a] NDE Research Group, Department of Mechanical Engineering, Imperial College London, SW7 2AZ, UK
[b] Rolls-Royce plc., Gipsy Patch Lane, Filton, Bristol, BS34 7QE, UK

A B S T R A C T

The use of nickel-based superalloys, such as Inconel 718, Udimet 720Li and Waspaloy, is widespread across the engineering industry due to their superior mechanical properties at elevated temperatures and excellent resistance to creep and fatigue under harsh working conditions. The microstructure of these materials, such as the precipitates and grain sizes, strongly influence the materials' performance. Currently, existing materials characterisation methods are time-consuming, costly and destructive, as well as only capable of taking measurements of surface or near-surface properties.

This paper presents a novel ultrasonic technique for bulk materials characterisation of nickel-based superalloys, based on a spherical harmonic convolution theory which has been successfully used to quantify texture in various metals; it is applied here to study a nickel-based superalloy, with a specific focus on the phase changes when subject to thermal loading. The key parameter used to interpret phase information of a material is the zeroth spherical harmonic coefficient of ultrasonic wave velocities, V_{00}, which corresponds to the average velocities across all directions in 3D space and is independent of crystallographic texture. Experimental investigation using samples of a representative material, Inconel 718, with contrasting microstructures, has shown a clear and quantifiable sensitivity of this coefficient to microstructural changes occurring within the material, and has thus laid the foundations for the development of a rapid phase characterisation technique for nickel-based superalloys using ultrasound.

1. Introduction

The development and subsequent advancement of nickel-based superalloys has been hugely beneficial across the engineering industry; their superior mechanical properties and resistance to creep, corrosion and oxidation at high operating temperatures has made them highly applicable in many different fields. Within aerospace, for example, the superalloys Inconel 718, Udimet 720Li and Waspaloy are often used within gas turbine engines in regions of extreme heat exposure [1–6]; and in the nuclear industry, the superalloy Inconel 82 is commonly used as a weld metal [7,8]. Due to the extensive use of these nickel-based superalloys, often for critical components, it is essential that the microstructure of the material is monitored and reliably characterised at any point in its lifecycle – whether it be during component fabrication and manufacture, or while in service – as any microstructural variations will have an impact on the material's performance. These variations could arise as a result of unpredictable stresses or strains under anomalous loading conditions, or exposure to higher temperatures than usual during service, if there is an 'overtemperature' incident; key indicators of such material degradation include grain size changes or dissolution of strengthening precipitates.

There are many examples of commonly utilised materials characterisation methods, such as microscopy-based techniques, of which there are a range of types available; these include scanning electron microscopy (SEM), electron backscatter diffraction (EBSD) and transmission electron microscopy (TEM). While they offer extremely high spatial resolution, these methods do have significant disadvantages; the preparation required to image samples is highly laborious, particularly for EBSD and TEM, and the time of inspection itself can also be lengthy to ensure all possible phase morphologies are captured [9]. Difficulties are often encountered in differentiating phases which have similar diffraction patterns [10]. The coverage area is also somewhat limited (in the order of tens of nm for EBSD [11]), due to the maximum sample size – particularly for TEM, where foils must be around 100 μm thick [12] (whereas SEM and EBSD can be used for up to 20 mm^2 samples). In terms of non-destructive techniques, there is the recently developed method of Spatially Resolved Acoustic Spectroscopy (SRAS), which uses surface acoustic wave velocity measurements to create a velocity map showing the orientation of grains [13,14]. However, this technique does also require preparation of the surface to very smooth finish, and the total

* Corresponding author.
** Corresponding author.
E-mail addresses: j.jobling18@imperial.ac.uk (J.H. Jobling), bo.lan@imperial.ac.uk (B. Lan).

https://doi.org/10.1016/j.ndteint.2024.103120
Received 24 January 2024; Received in revised form 2 April 2024; Accepted 14 April 2024
Available online 19 April 2024

time of inspection is still relatively long; its spatial resolution of around 20 μm means that it is also unable to resolve the phase information directly. If the access to the required facilities can be obtained, there are more powerful materials characterisation techniques available, such as neutron diffraction [15,16] and X-ray synchrotron measurements [17–19]. These are not without their limitations, however; as with the microscopy methods, size of a sample which can be inspected is limited, and very high energies are needed to penetrate larger volumes. There is also the additional challenge of acquiring access to these measurement facilities, due to the limited number available.

Due to the limitations of the various materials characterisation techniques, as discussed above, there is still the need for a non-destructive, inexpensive and rapid method to be developed for the bulk characterisation of material microstructure within the nickel-based superalloy family, to enable the reliable inspection of critical components across a broad range of engineering applications.

This work presents a new, rapid, non-destructive technique using ultrasonic wave speed measurements to characterise microstructure changes within nickel-based superalloys, based on a theoretical framework using a spherical harmonic expansion [20]. It was shown that the wave speeds in a polycrystal can be expressed as a convolution between the material texture and single crystal speeds; additionally, it was found that the zeroth order expansion coefficient of the polycrystal in this convolution, V_{00}, corresponds to the average wave speed across all 3D propagation directions; it only depends on the single crystal elastic constants and is independent of texture. It can therefore be used to estimate phase composition (as successfully demonstrated in a Ti-64 alloy [21]). This represents an excellent opportunity for the non-destructive testing (NDT) of engineering materials, such as the nickel-based superalloys, as any microstructural variations that occur are directly linked to (and can therefore indicate) any differences in mechanical properties or degradation, which could be detrimental to a critical component in service. The previously mentioned example of overtemperature exposure, due to abnormal operating conditions, can cause key strengthening precipitates to be dissolved back into solution, and/or a dramatic increase in grain size; both of these changes which would greatly impact the strength and fatigue resistance of a part. In addition, the change in the amount and type of precipitates would alter the single crystal elastic constants (SCECs), which would be detectable as a change in the wave speeds through the material. A reliable, non-destructive inspection technique with rapid feedback, which utilised this, would be a significant advantage in enabling a quick analysis of a component, to ensure that it was still suitable for use after such an occurrence while in service.

This paper will first briefly summarise the underlying theoretical framework of the spherical convolution theorem, with an emphasis on the key parameters required to extract phase composition estimates, before discussing the microstructure of Inconel 718, the material used for this initial study. The experimental methodology is then detailed, followed by the results from the 16 rounds of experiments completed, which show a clearly observable and quantifiable convergence to two very different V_{00} values depending on the sample's microstructure, and thus indicating that there is the potential for the spherical convolution technique to be developed for phase characterisation. Results from existing materials characterisation techniques (optical microscopy and SEM) have been used to corroborate the characterisation results from the ultrasonic wave speed measurement. There has also been some statistical analysis to quantify the uncertainties associated with the measurement system, and deduce the number of experiments required to reach a reliable conclusion. The paper concludes with a brief discussion of these results and error analysis, and outline future work to be undertaken in order to refine the technique for phase composition estimates within a nickel-based superalloy.

2. Methodology and materials

An overview of the underlying mathematics of the spherical convolution theory is presented here, with particular emphasis on the variables which are necessary in the estimation of phase composition; the microstructural characteristics of the material used for this study, Inconel 718, are also summarised. (For a more detailed description of the derivation process of the spherical convolution theory, the reader is directed to earlier publications [20–22].)

2.1. Spherical convolution theory

By assuming a polycrystalline aggregate is homogeneous such that, regardless of its direction, an acoustic wave always propagates through the same texture, the wave phase velocity variation function in 3D space (v) can be approximated by taking an average of the wave speeds along the propagation route at each point; the crystallographic orientation determines the speed at each point [21]. This velocity function can therefore be expressed as a spherical convolution between the ODF, ω, and the single crystal velocity variation function, k; the latter can be calculated from single crystal elastic constants (SCECs) of the material, widely available in the literature. This leads to the formulation of the fundamental equation of the theorem, where the spherical harmonic (SH) coefficients of the three functions satisfy a point-wise multiplication relationship, constituting a spherical harmonic expansion [20–22]:

$$V_{lm} = \sum_{n=-l}^{l} W_{lmn} K_{ln} \tag{1}$$

In terms of applying the spherical convolution towards characterising the microstructure of a material (in this case, through estimating the amount of each phase present), the main focus is on the velocity coefficient in equation (1), V_{lm}, but more specifically the zeroth order term V_{00}. These velocity coefficients are calculated using wave speeds in specific discrete evaluation directions as determined by the Gaussian-Legendre numerical integration scheme [20–22]:

$$V_{lm} = \frac{\pi}{N} \sum_{i=0}^{2N-1} \sum_{j=0}^{N-1} v(\theta_i, \varphi_j) Y_{lm}^{*}(\theta_i, \varphi_j) \omega_N \tag{2}$$

The order of the integration scheme is denoted N, with there being N number of discrete Gaussian-Legendre polar angles (or nodes), θ_i, and 2N equi-angular azimuthal angles from 0 to 2π, φ_j, in which the wave speeds must be measured. The conjugates of the SH bases for a given orientation (θ_i, φ_j) are represented as $Y_{lm}^{*}(\theta_i, \varphi_j)$, with ω_N giving the Gaussian weights of the nodes.

It has been found that a value of 6 for N is sufficient to achieve the required numerical accuracy [21] for the targeted truncation order of 4, which determines the 6 polar and 12 azimuthal directions for which the wave speeds are required – though using the antipodal symmetry of waves, this number can be halved. The experimental wave speeds measured in these discrete directions can then be used in the spherical convolution inversion process, in order to extract the spherical harmonic coefficients – and specifically the zeroth order velocity coefficient, V_{00}, which contains the phase information of the material.

2.1.1. Phase composition estimates

The fact that V_{00} is the specific coefficient containing the phase composition information of the material can be explained by examining how the three spherical harmonic terms in equation (1) of the zeroth order are linked:

$$V_{00} = W_{000} K_{00} \tag{3}$$

The spherical harmonic expansion can be thought of as analogous to the Fourier series, but for a spherical field; where the Fourier series expresses a periodic (or circular) function in terms of a sum of trigonometric functions, the spherical harmonics separates a spherical field into different shaped components, defined by specific orthogonal functions. An effective visualisation of these specific shapes can be found in

Ref. [23]. As with the Fourier series, where the first (or zeroth order) term is a constant, the zeroth order coefficient of velocity V_{00} will also be a constant for a given sample. The zeroth order term of the ODF, W_{000}, is always 1 regardless of texture, as it is analogous to taking the sum of all probabilities (of the orientation distribution function) over a spherical volume (as per the shape of the zeroth order spherical harmonic); in other words, averaging over all directions. As a result, the value of V_{00} is independent of texture, as any texture variations will not affect the term W_{000}; hence V_{00} will always be equal to the coefficient K_{00} of a single phase material. V_{00} is thus an intrinsic feature of that particular phase, reflecting its acoustic properties and being directly linked to the SCECs. The phase composition and presence (or absence) of various precipitates will alter the overall SCECs of the material, due to these precipitates also having their individual stiffnesses (and SCECs) which would contribute to that of the whole material; for example, if more of the stiffer precipitates were present, the SCECs of the overall material would be different than if none were present. These changes in the SCECs caused by the different phase amounts allows for this ultrasonic wave speed method to detect microstructural variations, that are spatially homogeneous on the macro-scale, which have occurred.

Developing this theory further for a dual phase material and using phases present in Inconel 718 after some specific processing (gamma, γ, and delta, δ) leads to the following expression:

$$V_{00}|_{overall} = V_{00}|_{\gamma}(h) + V_{00}|_{\delta}(1-h) \tag{4}$$

Here, h represents the volume fraction of the gamma phase present in the material. With the individual V_{00} values deduced from the phases' SCECs, together with the experimentally measured overall V_{00}, the volume fraction present of each phase can therefore be estimated. Previous estimates in the alpha percentage of dual-phase Ti–6Al–4V using this method with experimental data gave a volume fraction of 86.8 %, aligning well with the ~90 % of alpha phase reported in the literature [24,25] and showing promising results for the deployment of this technique. It should be noted, however, that the precision in the phase estimation using this method is dependent on the accuracies of the SCECs, and how far apart the V_{00} (or K_{00}) values of the individual phases are (where the larger the difference, the more accurate the estimation [21]) – as well as the experimentally measured V_{00} values. As far as the experimental V_{00} measurements are concerned, efforts can be made to refine the equipment and measurement acquisition; however, the data for specific phases' SCECs can prove more challenging. For precipitates with smaller morphologies, the measurement of the SCECs can be particularly difficult, as advanced (and often costly and time-consuming) techniques are required, such as nano-indentation or the use of X-ray synchrotron measurements; often these data are not available to find in the literature. Hence approximations may be necessary in the first instance (such as using image analysis of micrographs, together with hardness testing) until the SCECs can be measured using more accurate techniques.

Despite these limitations, however, the UWS technique still offers many advantages in contrast to existing microstructural characterisation techniques; not only in terms of its speed and ease of deployment, as previously discussed, but also the fact that the zeroth coefficient offers a statistical average measurement through the volume, rather than giving surface or sub-surface information. This therefore gives a better overall indication of the different phases which may be present within a nickel-based superalloy.

2.2. Microstructure of Inconel 718

Although the ultrasonic wave speed method has been applied to solely Inconel 718 thus far, this thought of as representative of other nickel-based superalloys, and hence the principles demonstrated are applicable across all materials within this family. Inconel 718 was the material with the easiest accessibility, as well as being of industrial interest due to its extensive use within aerospace engine components. The following section gives a brief summary of typical phases found within Inconel 718, in order to provide an understanding of the main precipitates present which could have an effect on ultrasonic measurements of the material, due to their impact on the overall SCECs.

The samples of Inconel 718 used for this investigation have been manufactured to the designation AMS 5662; the processing involves solution annealing at 968 °C, followed by a rapid cooling and finally a precipitation hardening at 718 °C for 8 h with furnace cool [26]. These processing steps allow the key strengthening precipitates, such as the gamma double prime, to form within the main gamma matrix.

2.2.1. Gamma and gamma phases

The main matrix phase in Inconel 718 is the gamma (γ) phase, formed of nickel and chromium crystallising in an FCC structure [27] – two of the main elements contributing to the corrosion resistance of the material. Niobium is added to form the major precipitation-strengthening component, the gamma double prime (γ'') phase [27]; this is a meta-stable phase with a body-centred tetragonal (BCT, or $D0_{22}$) structure and chemical composition Ni_3Nb [28]. Titanium and aluminium are added to the superalloy melt to facilitate the formation of the gamma prime (γ′) precipitate, an intermetallic compound with chemical composition $Ni_3(Ti,Al)$ [27]. The γ′ precipitate has a simple cubic crystal structure which is $L1_2$ ordered, and has a lower hardening effect than the γ'' particles – the volume fraction of this phase is typically less than 5 % [29], though they do still offer a small degree of strengthening [30].

2.2.2. Delta phase

The delta (δ) phase is an intermetallic compound of formula Ni_3Nb and an orthorhombic structure [27]; it generally forms as a long, needle-like (or plate-like) shape along the γ phase grain boundaries [31]. The growth of the δ phase tends to correspond to a loss of the γ'' phase – an undesired effect, as the δ phase does not contribute significantly to the hardening of the alloy, and its presence in fact implies loss of hardenability due to the depletion of the γ'' phase. It has also been associated with causing increased susceptibility to hot cracking [32] and increased plasticity [33].

2.2.3. Carbides and other minor phases

The addition of carbon to the superalloy melt during Inconel 718 fabrication results in the formation of precipitates of the form MC, with M denoting a metal (titanium or niobium in this case [27]). These are insoluble segregates, and tend to reduce strength and ductility. As carbide phases are slightly more difficult to reveal during the etching process required for microscopy, they can often be masked and confused with those of the Laves phase [34], a precipitate typically high in niobium, molybdenum and nickel, with smaller quantities of iron, chromium and titanium. Similar to the δ phase, the Laves phase has also been found to affect the ageing response of Inconel 718 [34].

3. Summary

To summarise, there are several precipitates present within Inconel 718 which could affect the mechanical behaviour (and therefore ultrasonic characteristics) of the material, depending on the amount and properties of each phase present; in particular, the proportion of different particles present, such as the γ'' phase, will alter the overall SCECs of the material. This is one fundamental reason that the ultrasonic wave speed method is able to detect microstructural changes within the material. Currently, one of the main difficulties in observing microstructural changes is due to the fact that many of these phases are very difficult to image and identify; for example, the length scale of the γ'' phase is around 20 nm [35], beyond the resolution of many powerful microscopes. The development of an ultrasonic wave speed measurement technique would allow for a much more rapid and reliable bulk

material assessment of any phase composition changes which had occurred, without the need for extensive preparation or being affected by any microstructural homogeneities within the material.

4. Experiments: Procedure and results

4.1. Experimental procedure

The following section will cover all steps in the experimental process for this investigation, describing first the experimental platform used to acquire the ultrasonic signals required to calculate the zeroth coefficient of velocity, before describing the samples undergoing testing. The preparation steps required for microscopy, to verify that the microstructural changes had taken place after heat treatment, have also been included.

4.1.1. Ultrasonic wave speed measurement: experimental platform

For the ultrasonic wave speed measurements, an ultrasonic water tank adapted from previous studies was used [21,35,36], built to enable the straightforward and semi-automated measurement of the ultrasonic wave speeds in all of the required directions for the spherical convolution theory. The design is based on a conventional ultrasonic water tank used for inspection in the Non-Destructive Evaluation (NDE) field, and a schematic of the setup with detailed description of the experimental procedures can be found in Ref. [21]. The sample is submerged in water parallel to and above an acoustic mirror, with a piezoelectric transducer suspended above the water and pointing directly normal to both. This transducer is a transmitter-receiver, sending ultrasonic waves through the sample and receiving the double-through-transmission signals; these waves have passed through the sample and reflected back off the acoustic mirror, and ensure that the macro-texture being inspected is an average across the volumetric region of interest, or VROI [21]. The VROI is around 5 times the thickness of the part, as determined by the largest angle of the Gaussian-Legendre nodes, and is assumed to be homogeneous (as validated from previous experiments [21]). The tilting of the sample is done automatically, as is the alignment of the sample to be parallel to the transducer; the operator is only required to rotate the sample by 30° to capture the signals in the 6 different directions as determined by the convolution theory.

4.1.2. Test samples and heat treatment conditions

Four samples of Inconel 718 were machined into ~5 mm thick, 120 mm wide dodecagons; this was to make the angle of rotation of the sample in each of the required orientations easy to identify when carrying out the experiment. Two of these were subjected to a heat treatment programme of a hold at 1100 °C for 4 h, followed by an oil quench (for a rapid cool), to allow for all precipitates within the samples to be drawn back into solution. The schematic of the heat treatment procedure is illustrated in Fig. 1. Following this, small 5 mm-cube specimens were machined off each dodecagon to prepare for observation with a scanning electron microscope; after mounting in conductive Bakelite, silicon carbide papers were used to grind the surface before using 6 μm, 3 μm and 1 μm diamond suspension solution and OPS to polish. They were then etched using a solution of 1 % ammonium sulphate, 1 % citric acid, at 4 V for 20 s s, before observation with optical and scanning electron microscopy.

4.2. Optical and scanning electron microscopy

Fig. 2a and b shows the optical microscopy images obtained of one of the samples in the as-received condition as well as one after heat damage had occurred. It is immediately apparent that, as well as there being the absence of precipitates, there has also been significant grain growth after the heat treatment has taken place; the absence of the δ phase (the needles on the grain boundaries seen in Fig. 2a) has allowed the grains to grow without being inhibited by the pinning effect that this precipitate

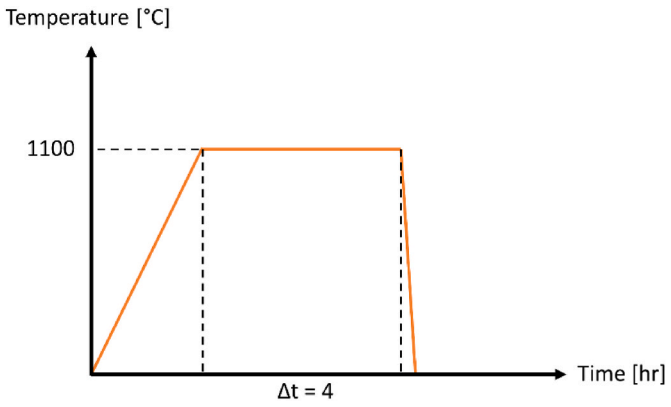

Fig. 1. Time-temperature diagram for heat treatment process, simulating heat damage of Inconel 718. As the procedure was carried out at an external facility, the total ramp up time of the furnace to temperature is unknown; however, documentation provided confirms the sample was held at temperature for the required 4 h.

provides, and also makes it much more difficult to distinguish between the various grains with nothing to delineate the boundaries. Micrographs obtained with SEM show the contrasting grains slightly clearer and have also been included as Fig. 3a and b. As the δ phase has a higher stiffness than the overall γ matrix, the dissolution of this phase after the heat treatment will affect the SCECs of the material, and it will have a lower overall stiffness; this should, in theory, result in lower wave speeds through the material, detectable by having a lower zeroth coefficient of velocity, V_{00}.

The heat treatment was indeed very successful in generating a greatly contrasting microstructure, and thus the work could begin on ultrasonic water tank measurements. Initially, a 10 MHz frequency transducer was used to capture the required ultrasonic signals – this had previously been found suitable for titanium alloys; the wavelengths are typically over 10 times the grain sizes, minimising scattering and achieving good signal to noise ratios of around 40 dB and above [21]. However, the drastic increase in grain growth following the heat treatment resulted in a significantly higher level of attenuation, with the double through-transmission signal not being detectable; hence the frequency was dropped to 5 MHz for the heat damaged, or 'HD', samples. This was also an excellent demonstration of one of the advantages of this technique; in terms of the underlying theory, the fact it is dimensionless means that the change of frequency should have no effect on the calculation of the V_{00} coefficient, or create additional errors; the disadvantage is the loss of temporal resolution as a result of the reduced frequency, but as it is only the peaks of the waveforms being used in the cross-correlation process this should not affect the final calculated data. (However, as best practice, the highest possible measurement frequency should be used for the best temporal resolution.)

4.3. Zeroth coefficient results

In total, each of the 4 samples was tested 16 times; each 'test' consisted of three runs of the measurement acquisition process, from which an average was taken. Fig. 4 shows the cumulative mean zeroth coefficient values for each sample plotted with the number of experiments carried out. It can be seen that there is a clear convergence for the V_{00} of each sample, as well as a noticeable difference between the categories of sample conditions tested – the as-received and the heat damaged (or HD) samples – due to the relatively small wave speed differences being on the same level as random experimental errors. This convergence from the repeated tests proves both the error and the wave speed difference, and values for each sample set are remarkably similar to each other; OG1HD and OG2HD both converge to a mean of 5.7442×10^3 m/s, with OG3

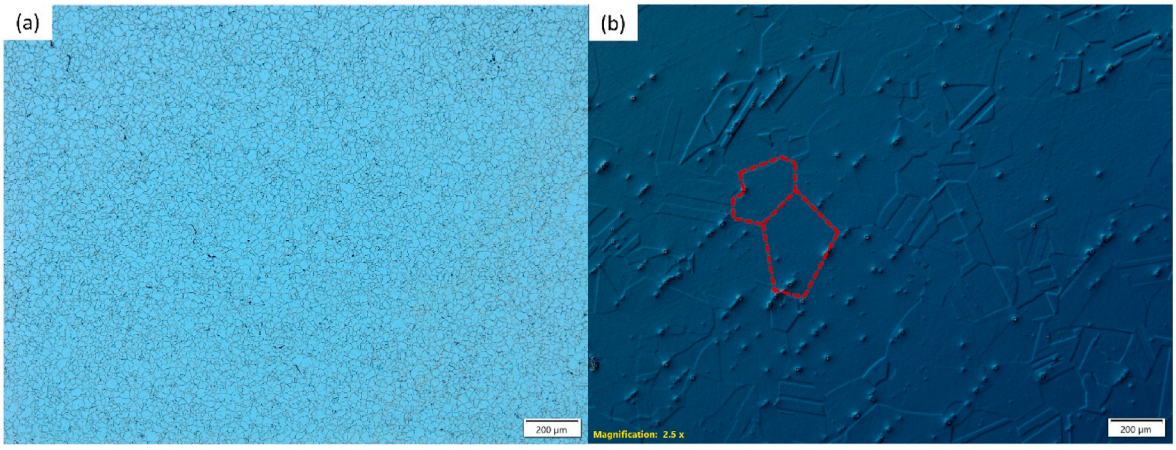

Fig. 2. Optical images of samples (a) as received and (b) after heat damage (with grains outlined in red for clarity). The delta phase can be seen before heat damage as the black 'needles' delineating the grains, and are absent after heat damage has occurred. The γ′ and γ′′ phases are beyond the resolution of the microscope. (For interpretation of the references to colour in this figure legend, the reader is referred to the Web version of this article.)

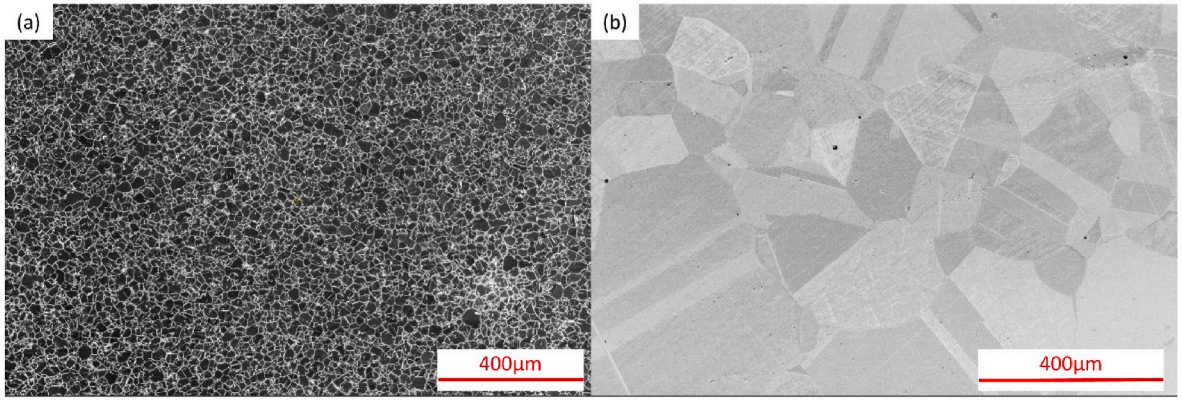

Fig. 3. SEM images of samples (a) as received and (b) after heat damage. The delta phase is now seen in white for the as-received sample, and are absent after heat damage as occurred. Again, the γ′ and γ′′ phases are beyond the resolution of the SEM.

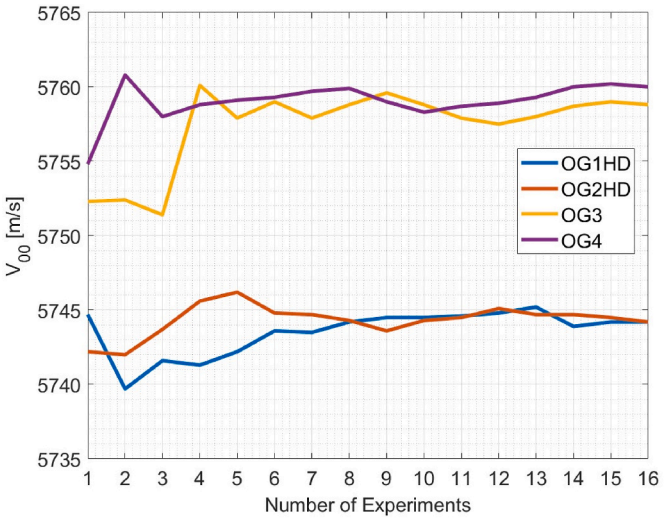

Fig. 4. Cumulative mean values of V00 for each sample.

and OG4 converging to 5.7588×10^3 and 5.7600×10^3 m/s respectively, just 1.2 m/s apart. The difference in the values after heat damage has occurred is also very noticeable – around 15 m/s, which is above the error of typical ultrasonic measurements [21]. Although in percentage terms, the difference in V_{00} between the two categories of sample is small, this is unavoidable as the wave speeds in nickel-based superalloys are 3 orders of magnitude larger than the error level of ultrasonic measurements. It should be emphasised that, for this UWS technique, the absolute wave measurements are key; the fact that there is a noticeable difference between the converged V_{00} values for each sample has demonstrated the effectiveness of this method in detecting microstructural changes. Hence these results provide clear evidence that, from cross comparison with the micrographs obtained, the spherical harmonic zeroth coefficient of velocity is indeed sensitive to microstructure changes within the material.

4.4. 3.4 pole figures

In order to demonstrate the benefit of the method with regards to its independence of textural variations, pole figures generated for each sample through the deconvolution process (using the MTEX MATLAB extension) have been included here in Fig. 5, for both 111 and 200 orientations. The intensities of the plots correspond to the prevalence of the preferred orientations within the sample. It can be seen that each sample has a very different texture, and yet – particularly with the heat damaged samples – this difference has not manifested itself at all in changes with the zeroth coefficient. This therefore proves that it is purely chemical changes within the material which would affect the zeroth coefficient, further reinforcing the strength of the method. A further point to note is that these pole figures show the textures in the

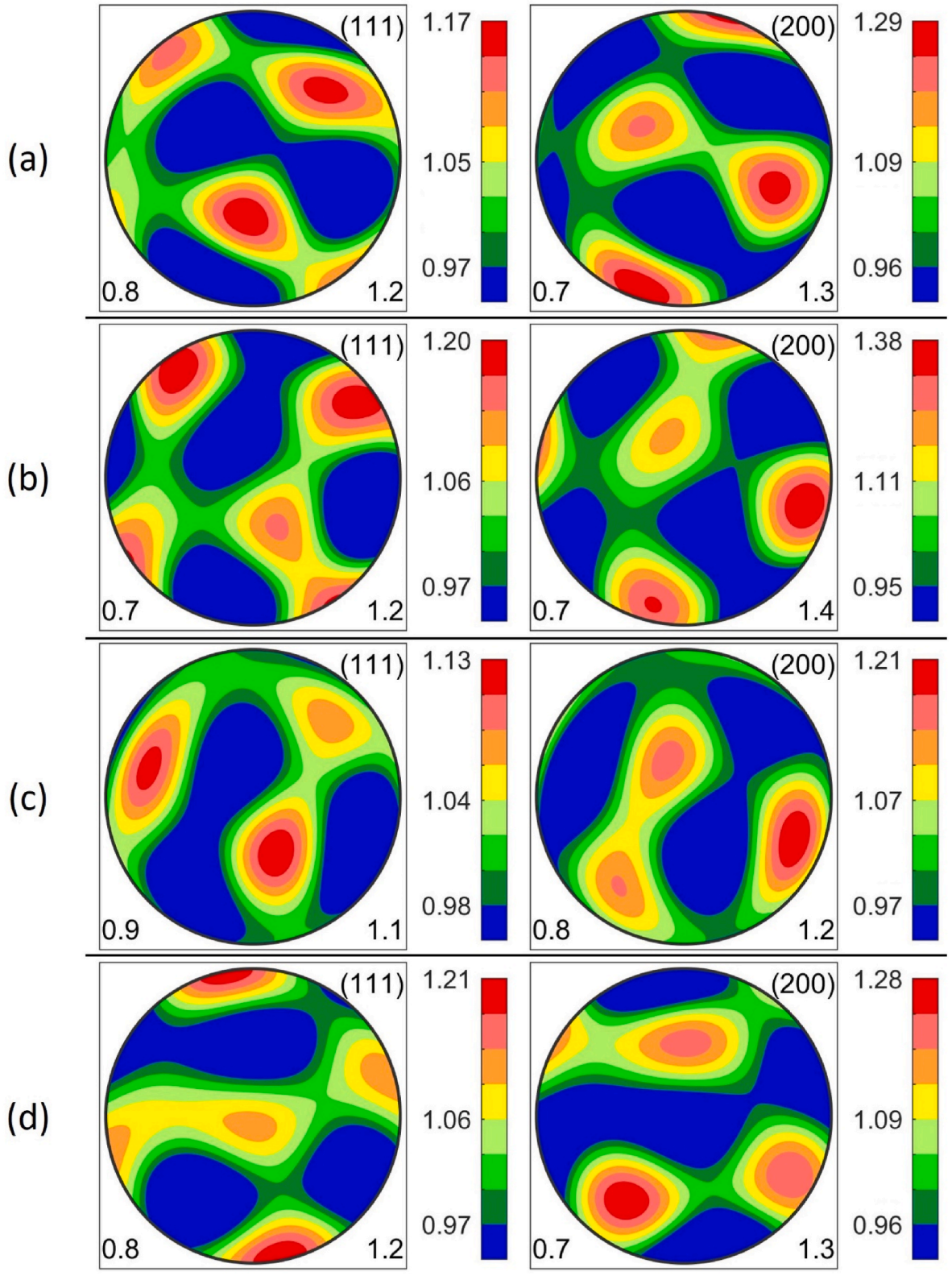

Fig. 5. Pole figures in the 111 and 200 orientations for (a) OG1HD, (b) OG2HD, (c) OG3 and (d) OG4.

samples are relatively random; however, even if the inspection method was applied to a material with strong texture, such as a forged component, it would still be possible to detect microstructural changes via the zeroth coefficient measurements with no influence caused by texture; as discussed in Section 2, V_{00} is related to the single crystal elastic properties, and the texture has no effect on the polycrystal data.

4.5. Error analysis of wave speed measurement platform

Although the data in Fig. 3 show a clear convergence in the as-received and heat damaged conditions, which can be robustly differentiated, it is clear that there exists a level of experimental error which masks the true convergence at a low number of tests, but is averaged out

at a higher number of tests. It should be emphasised that the differences in wave speeds (at the level of 15 m/s) are relatively small, and comparable to experimental error levels; this is part of the reason why averaging works well in this case. The convergence process can be used to analyse both the real data required from the experiment, as well as the associated errors of the experimental platform. This analysis method itself does not depend on the platform, and can thus determine the number of tests required to achieve a certain confidence level.

To carry out the statistical analysis to attempt to quantify the convergence results, the experimental data for each sample was randomised ten times to vary the order in which the mean is calculated, to ensure that the number of trials after which convergence is reached is consistent. The 95 % and 98 % confidence intervals were calculated using the parameters from a fitted Gaussian distribution; these intervals describe the probability that a measurement would fall between these ranges of values. The distributions are shown in Fig. 6 for each sample, and the average number of trials required for each sample to reach the 95 % and 98 % confidence intervals for the ten permutations is shown in Fig. 7.

The statistical analysis has been carried out assuming that the experimental errors follow a Gaussian distribution, which is a well-accepted means for such analyses of a dataset with white noise, or random error [36–38]. However, from the histograms shown in Fig. 6, it is apparent that there are some outliers from the fitted Gaussian distributions – in particular for samples OG1HD and OG3. The use of this distribution assumes the experiments to be a random process, whereas in reality more tests may be required than those carried out here for this to adequately manifest; there may also be other, more systematic errors occurring. However, we have not seen evidence to convince us that there is any other systematic error other than white noise which has contributed to the distribution of the results, nor could we reach any conclusive quantification, despite our best efforts; hence, even with the outlying data, the Gaussian distribution has still been considered the best approximation for measurement and instrumental errors for these results, and has subsequently allowed for the estimation of confidence levels for the experimental data. The deviation of data from the standard

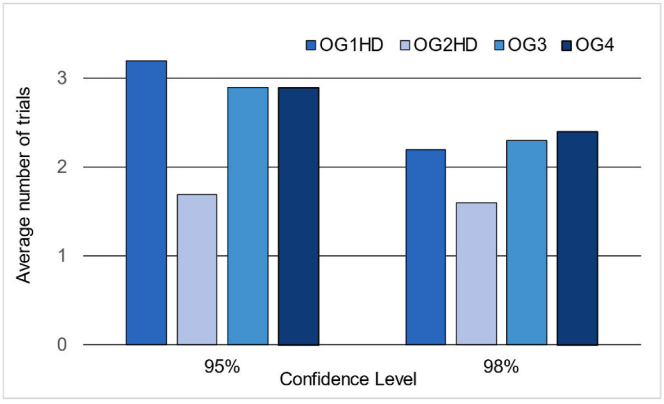

Fig. 7. Average number of trials across 10 randomised permutations to reach 95 % and 98 % confidence intervals.

model is most likely due to the relatively small sample set, due to time constraints; for these material conditions, ideally the largest possible number of tests (and subsequent analysis of the averages) would be carried out, as the velocity differences between the two groups of samples is less than 15 m/s – within the reasonable error bounds for immersion ultrasonic measurements.

It can be seen that, in the worst case, the cumulative mean is within the 95 % confidence interval after four trials. In addition, convergence to within 2 m/s of the mean value is observed after 8 experiments (see Fig. 4), implying that a conclusive result with regards to the microstructure can be attained after this number of trials for this particular experimental configuration. However, it was also observed that the confidence intervals vary in width between each of the samples; further investigation is required to determine the cause of these discrepancies, and is beyond the scope of this paper.

Despite there being a number of different factors which could cause errors in measurements (as with any experimental measurement) including small vibrations of the equipment and the water level of the

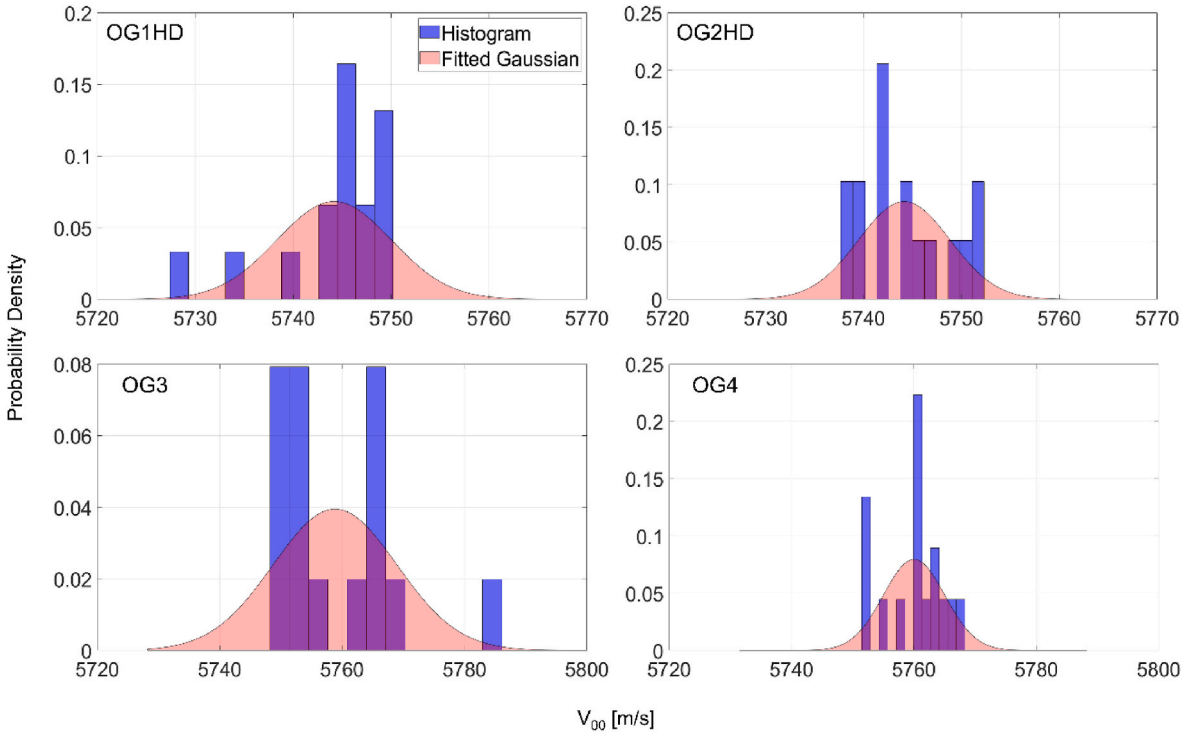

Fig. 6. Fitted Gaussian distributions for experimental data from each sample.

tank, it is important to consider that – as previously mentioned – the differences being detected in ultrasonic wave speeds are relatively small for this material. The inevitable experimental errors which arise are also themselves extremely small, and will average out due to being a random parameter (which is what has been observed). Hence, despite these experimental uncertainties, it can be concluded that a set of 8 trials per sample will be sufficient for this particular platform to reach a converged value of zeroth coefficient, and allow for a deduction to be made regarding the microstructural characteristics of the material.

5. Discussion

Using the ultrasound water tank setup, the sensitivity of the zeroth order spherical harmonic coefficient (V_{00}) to microstructural changes occurring within nickel-based superalloys has been investigated, and the experimental evidence has shown conclusively that this measurement technique is able to detect whether changes have occurred. The samples which were subjected to heat damage had a noticeably lower value, consistent with the fact that the V_{00} essentially represents the average of 3D wave speeds in all propagation directions throughout the material, and thus an absence of strengthening and stiffening precipitates within the sample will therefore result in lower overall wave speeds. The positive result of this study has indicated that the technique could be developed further towards quantifying the phase compositions within the material, for which the coefficient V_{00} is key.

Having demonstrated that the V_{00} is sensitive to changes in microstructure, the next stage will be to apply these measurements to the phase composition estimation within Inconel 718. Although in terms of industrial benefit, the application of the method towards estimating the amount of γ'' and γ' phases would be of most use (due to their being the main precipitates contributing to the strengthening of the material), it has been found that the delta phase is much more straightforward to manipulate; from the time-temperature-transformation (TTT) for Inconel 718 [39], it can be seen that there is a region beyond a certain hold time and temperature at which, if the material is held, only the delta phase should be present, and hence result in a dual-phase material. There is the additional advantage of this precipitate being much more straightforward to image than the γ' or γ'' phases using SEM, which would be required to validate the accuracy of phase composition estimates using the UWS method. The main challenge with regards to the phase estimation process is the lack of available data for the SCECs of the delta phase; further investigation will be carried out in order to either measure these using experimental techniques such as nano-indentation, or to estimate the K_{00} of the delta phase directly via Equation (4) using existing sample micrographs and corresponding V_{00} data.

Once developed further for phase estimation, this characterisation system would have numerous advantages to both research and industry applications, particularly in terms of inspection efficiency. Although currently the system requires some user adjustment, a fully automated version (currently near completion) would enable the full inspection of a sample in a matter of minutes – a significant time saving compared to the sample preparation and analysis procedure required for current microscopy methods in use. There is also very rapid feedback of results after testing, due to the simplicity and speed of the deconvolution process, and once the uncertainty of the particular test setup has been quantified, the number of tests required for a conclusive result can be deduced and applied to any sample being examined. Improvement in efficiency is not just in terms of time taken, but also regarding cost; the components required to assemble this test system are inexpensive and very easily accessible, allowing for the spherical convolution method to be deployed in research laboratories as well as on manufacturing production lines – and as the underlying theory is dimensionless, the scales required for a particular application can be adjusted accordingly with no change to the post-processing procedure.

The dimensionless theory also has further implications – as well as being scalable in terms of physical scale, the technique can be applied across the frequency spectrum (as demonstrated here, due to the lower frequency required for heat damaged sample measurements). One of the limitations of the method in its current configuration is that there is the need for parallelism of the sample surface, and thus more complex geometries cannot yet be inspected. There is also a size limit for samples compatible with this water tank, as beyond a ~15 mm specimen thickness other internal reflections begin to appear, which interfere with the capture of the main double through-transmission signals. However, other emerging techniques, such as laser ultrasound excitation, laser interferometer reception or resonant ultrasound spectroscopy, could negate the need for a piezoelectric transducer and thus enable a more flexible approach to inspection. It should also be noted that the size limitation is not for the characterisation method as a whole, but just of this particular test rig; ultrasound equipment commonly in use can easily evaluate materials of much greater thicknesses, often greater than 50 mm, than the limit of ~10 mm for neutron or X-ray synchrotron measurements [21]. Hence the deployment of this ultrasonic technique would enable bulk material characterisation of much larger volumes.

A further advantage of this technique is the independence of the zeroth coefficient to any changes within materials except for chemical alterations; this means that any difference in values observed is an indication of changes in its chemistry, something which varies depending on whether a precipitate (or precipitates) have gone into or come out of solution, rather than any other modifications such as textural variation. This has been demonstrated with the results of this investigation.

The ultrasonic spherical convolution technique is not limited to applications within the materials characterisation field, but could also be developed as an alternative to the monitoring of in-service components, particularly if adapted to be used with alternative ultrasonic configurations (such as the previously mentioned laser techniques). Fatigue life monitoring is of particular interest, currently carried out using hardness testing; although this is, in theory, a non-destructive technique, the polishing of the material surface in preparation for the testing is not only time-consuming but can also increase the risk of crack propagation. Fatigue performance is very closely linked to grain size, which in turn affects the attenuation characteristics of a material; as seen from the samples in this investigation, components exposed to overtemperature conditions will see a huge increase in grain size, which increases the ultrasonic attenuation observed. From this behaviour alone, it can be inferred that a microstructural change has taken place, and if required further investigation in terms of characterising what changes have occurred can be carried out. The deployment of the ultrasonic spherical convolution technique in this case would enable a much more rapid assessment of the part without any surface preparation, hence minimising any risk of damage and considerably reducing the overall time of inspection. In the future, this technique may also be employed to identify changes in microstructure from overtemperature events, that would otherwise require metallography or hardness testing (where the latter can lead to fatigue initiation sites).

6. Conclusions

The ultrasonic spherical harmonic convolution technique, previously used to measure texture in hexagonal and cubic materials, has been proved to be sensitive to microstructure changes occurring within nickel-based superalloys. Samples of a representative material, Inconel 718 (in both as-received and heat damaged conditions), were used to obtain ultrasonic wave speed measurements. A spherical deconvolution inversion was used to extract the zeroth order coefficient of velocity, V_{00}, from these measurements, the key variable within which the phase information of the material is contained. It was proved that there was a clear and quantifiable difference between the zeroth coefficient of samples depending on their microstructure (which had drastically changed after heat damage, as verified with optical microscopy and

SEM); the heat damaged samples exhibited much lower values, consistent with the lack of strengthening and stiffening precipitates resulting in much lower wave speeds. Statistical analysis on the full set of experimental results also allowed for the uncertainty in the ultrasonic setup to be quantified, and it has been determined that conclusive results can be obtained (with good convergence to the mean value) after around 8 experimental trials. The positive outcome from this feasibility study, showing that the zeroth coefficient of velocity is indeed sensitive to the microstructure within nickel-based superalloys, has paved the way for further studies using Inconel 718 to begin applying the method towards predicting the phase compositions of different precipitates within the material, and develop a rapid, inexpensive and non-destructive tool for both research and industrial applications, such as metallurgy monitoring and tailored component fabrication.

CRediT authorship contribution statement

Jennifer H. Jobling: Writing – original draft, Investigation, Formal analysis, Data curation. **Edward A. Saunders:** Writing – review & editing, Supervision, Resources, Investigation, Data curation. **Tim Barden:** Supervision. **Michael J.S. Lowe:** Writing – review & editing, Supervision. **Bo Lan:** Writing – review & editing, Supervision, Software, Resources, Methodology, Conceptualization.

Declaration of competing interest

The authors declare that they have no known competing financial interests or personal relationships that could have appeared to influence the work reported in this paper.

Data availability

Data will be made available on request.

Acknowledgements

The authors would like to thank EPSRC (EP/L015587/1) and Rolls-Royce plc for the funding for this project, Antonio de Sanctis for assistance with experimental equipment, Dr Ming Huang for advice regarding statistical analysis, André Lello for mathematical discussions (all of Imperial College London), and Nicholas Calcutt and Dr Mark Hardy of Rolls-Royce for discussions on nickel-based superalloys. BL wishes to acknowledge the support from the Imperial College Research Fellowship Scheme.

References

[1] Reed RC. The superalloys: fundamentals and applications. Cambridge: Cambridge University Press; 2008.
[2] Amiri A, Bruschi S, Hossein Sadeghi M, Bariani P. Investigation on hot deformation behavior of Waspaloy. Mater Sci Eng 2013;562:77–82.
[3] Utada S, Sasaki R, Reed RC, Tang YT. Overheating of Waspaloy: effect of cooling rate on flow stress behavior. Mater Des 2022;221:110911.
[4] Liu F, Chen J, Dong J, Zhang M, Yao Z. The hot deformation behaviors of coarse, fine and mixed grain for Udimet 720Li superalloy. Mater Sci Eng 2016;651:102–15.
[5] Chang L, Jin H, Sun W. Solidification behavior of Ni-base superalloy Udimet 720Li. J Alloys Compd 2015;653:266–70.
[6] Jackson MP, Reed RC. Heat treatment of UDIMET 720Li: the effect of microstructure on properties. Mater Sci Eng 1999;259(1):85–97.
[7] Jang C, Lee J, Kim JS, Jin TE. Mechanical property variation within Inconel 82/182 dissimilar metal weld between low alloy steel and 316 stainless steel. Int J Pres Ves Pip 2008;85(9):635–46.
[8] Panneerselvam G, Raju S, Jose R, Sivasubramanian K, Divakar R, Mohandas E, Antony MP. A study on the thermal expansion characteristics of Inconel-82® filler wire by high temperature X-ray diffraction. Mater Lett 2004;58(1–2):216–21.
[9] Szczotok A. Quantitative evaluation of carbides in nickel-base superalloy MAR-M247. IOP conference series: materials science and engineering, vol. 22; 2011, 012007.
[10] Sharma J, Nicolay A, De Graef M, Bozzolo N. Phase discrimination between δ and η phases in the new nickel-based superalloy VDM Alloy 780 using EBSD. Mater Char 2021;176:111105.
[11] Charpagne M-A, Vennegues P, Billot T, Franchets J-M, Bozzolo N. Evidence of multimicrometric coherentγ'precipitatesin a hot-forgedγ–γ′nickel-based superalloy. J Microsc 2016;263(1):106–12.
[12] Parsa AB, Ramsperger M, Kostka A, Somsen C, Korner C, Eggeler G. Transmission electron microscopy of a CMSX-4 Ni-base superalloy produced by selective electron Beam melting. Metals 2016;6(11):258.
[13] Sharples S, Clark M, Somekh MG. Spatially resolved acoustic spectroscopy for fast noncontact imaging of material microstructure. Opt Express 2006;14:10435–40.
[14] Clark M, Sharples SD, Somekh MG. Fast, all-optical Rayleigh wave microscope imaging on isotropic and anisotropic materials. IEEE Trans Ultrason Ferroelectrics Freq Control 2000;47(1):65–74.
[15] Turner RP, Panwisawas C, Lu Y, Dhiman I, Basoalto HC, Brooks JW. Neutron tomography methods applied to a nickel-based superalloy additive manufacture build. Mater Lett 2018;230:109–12.
[16] Grant BMB, Francis EM, Quinta da Fonseca J, Daymond MR, Preuss M. Deformation behaviour of an advanced nickel-based superalloy studied by neutron diffraction and electron microscopy. Acta Mater 2012;60(19):6829–41.
[17] Link T, Zabler S, Epishin A, Haibel A, Bansal TX. Synchrotron tomography of porosity in single-crystal nickel-base superalloys. Mater Sci Eng 2006;425(1–2):47–54.
[18] Epishin A, Camin B, Hansen L, Chyrkin A, Nolze G. Synchrotron sub-μ X-ray tomography of Kirkendall porosity in a Diffusion Couple of nickel-base superalloy and nickel after annealing at 1250C. Adv Eng Mater 2021;23:2001220.
[19] le Graverend J-B, Jacques A, Cormier J, Ferry O, Schenk T, Mendez J. Creep of a nickel-based single-crystal superalloy during very high-temperature jumps followed by synchrotron X-ray diffraction. Acta Mater 2015;84:65–79.
[20] Lan B, Dunne FPE, Lowe MJS. A generalized spherical harmonic deconvolution to obtain texture of cubic materials from ultrasonic wave speed. J Mech Phys Solid 2015;83:221–42.
[21] Lan B, Britton TB, Jun T-S, Gan W, Hofmann M, Dunne FPE, Lowe MJS. Direct volumetric measurement of crystallographic texture using acoustic waves. Acta Mater 2018;159:384–94.
[22] Lan B, Dunne FPE, Lowe MJS. A spherical harmonic approach for the determination of HCP texture from ultrasound: a solution to the inverse problem. J Mech Phys Solid 2015;83:179–98.
[23] Weisstein EW. Spherical harmonic. Wolfram Research, Inc.; 2024 [Online]. Available: https://mathworld.wolfram.com/SphericalHarmonic.html. [Accessed 12 March 2024].
[24] Warwick JLW, Coakley J, Raghunathan SL, Talling RJ, Dye D. Effect of texture on load partitioning in Ti-6Al-4V. Acta Mater 2012;60(10):4117–217.
[25] Williams JC, Lutjering G. Titanium matrix Composites. In: Titanium. Engineering materials, Processes. Berlin: Springer; 2007. p. 367–82.
[26] Tech Steel & Materials. Nickel Inconel 718 AMS 5662. Tech Steel & Materials; 2022 [Online]. Available: https://www.techsteel.net/alloy/nickel/inconel-718/ams-5662. [Accessed 23 May 2022].
[27] Thomas A, El-Wahabi M, Cabrera JM, Prado JM. High temperature deformation of Inconel 718. J Mater Process Technol 2006;177:469–72.
[28] Paulonis DF, Oblak JM, Duvall DS. Precipitation in nickel-based alloy 718, vol. 62. American Society of Metals; 1969. p. 611–22.
[29] Huang Y, Langdon TG. The evolution of delta-phase in a superplastic Inconel 718 alloy. J Mater Sci 2007;42:421–7.
[30] Slama C, Servant C, Cizeron GJ. Aging of the Inconel 718 alloy between 500 and 750°C. J Mater Res 1997;12:2298–316.
[31] Loria EJ. The status and prospects of Alloy 718. J Met 1988;40:36–41.
[32] Lu Q. HAZ Microstructural evolution in alloy 718 after multiple repair and PWHT cycles. Ohio: Ohio State University; 1999. PhD thesis.
[33] Ning Y, Huang S, Fu MW, Dong J. Microstructural characterisation, formation mecha-nism and fracture behavior of the needle δ phase in Fe-Ni-Cr type superalloys with high Nb content. Mater Char 2015;109:36–42.
[34] Eiselstein HL. Metallurgy of Columbium-Hardened nickel-chromium-iron alloy. Advances in the Technology of Stainless Steel and Related Alloys 1965;369:62–77.
[35] Orozco-Caballero A, Gutierrez C, Gan B, Molina-Aldareguia JM. High-throughput nanoindentation mapping of cast IN718 nickel-based superalloys: influence of the Nb concentration. J Mater Res 2021;36:2213–22.
[36] Leo WR. Techniques for nuclear and particle Physics experiments. Berlin: Springer; 1994.
[37] Hodges L. Common Univariate distributions. In: Statistical methods for physical Science. San Diego, CA: Academic Press; 1994. p. 35–61.
[38] Siegel AF. Practical Business Statistics. Amsterdam: Academic Press; 2011.
[39] Oradei-Basile A, Radavich JF. A current T-T-T diagram for wrought alloy 718. Superalloys 718, 625 and various Derivatives, vol. 1991. Warrendale, PA: The Minerals, Metals & Materials Society; 1991. p. 325–35.